

Investigation of Sputter-Deposited Thin Films of Lithium Phosphorous Sulfuric Oxynitride (LiPSON) as Solid Electrolyte for Electrochromic Devices

Christian Lupo, Fabian Michel, Florian Kuhl, Yurong Su, Martin Becker, Angelika Polity, and Derck Schlettwein*

Lithium phosphorus sulfuric oxide nitride (LiPSON) prepared by radio frequency sputtering is investigated as a transparent solid lithium-ion conductor for use in all-solid-state electrochromic (EC) devices. The LiPSON layers are characterized by X-ray photoelectron spectroscopy (XPS) and their electrical characteristics are studied by temperature-dependent impedance spectroscopy. Half-cells of LiPSON deposited on tungsten oxide (WO_x) in contact with 1 M LiClO_4 in propylene carbonate are studied by electrochemical impedance spectroscopy (EIS) and spectroelectrochemical measurements by cyclic voltammetry and chronoamperometry. A significant influence of LiPSON deposition conditions on the EC characteristics of WO_x is observed in the achievable transparency change, as well as the color impression in the bleached and colored state. Formation of a solid–electrolyte interface (SEI) is indicated that leads to poor EC performance with long switching times of 20–60 min. Appropriate deposition conditions for LiPSON are established that maintain a good EC activity of WO_x . An all-solid-state EC device is assembled of WO_x /LiPSON with vanadium titanium oxide as counter electrode and aluminum-doped zinc oxide as back contact. Temperature-dependent EIS and spectroelectrochemical measurements show that in such an all-solid-state stack, the detrimental contact resistance could be avoided and switching times of less than 60 s are achieved.

1. Introduction


Established electrochromic (EC) devices consist of a cathodically coloring material (mostly tungsten oxide, WO_x), a liquid or polymeric gel electrolyte, and an anodically coloring or noncoloring counter layer, all sandwiched between transparent conducting oxide (TCO) layers and glass.^[1] The electrolyte is a crucial component for functionality and safety, a short circuit by a conducting path through it, for example, can damage the whole device. The current standard polymeric gel electrolyte in commercial smart windows based on WO_x can lead to long-term instability by delamination and shrinkage.^[2–4] As an alternative, solid electrolytes already have reached considerable attention in the research and development of all-solid-state thin-film batteries because of significant advantages compared with liquid or polymer-based electrolytes.^[5,6] Without a liquid component, elaborate device sealing is not needed and packaging can be simplified.^[7,8]

Furthermore, solid inorganic electrolytes provide a high mechanical and thermal stability, which can be of considerable advantage also when used in large-area EC windows.^[6,9] Another benefit is provided by an improved electrochemical stability under conditions of changing temperatures from day to night and from summer to winter in combination with altered solar radiation.^[9]

Among appropriate inorganic solid electrolytes, lithium phosphorous oxynitride (LiPON) can be considered a well-established material for use in batteries and EC devices.^[10–17] LiPON-based electrolytes show great potential to improve several characteristics of devices because of the inherent safety, fast charge transport, good thermal, and outstanding mechanical stability.^[10,18] Modifications of LiPON with different additional elements were tested to improve specific characteristics of pure LiPON thin films.^[19] Recently, modified versions of LiPON containing silicon (LiSiPON) or sulfur (LiPSO) with improved electronic characteristics were introduced.^[20,21] In LiSiPON, ionic conductivity increased with increasing silicon content but the transparency in the range of visible light decreased significantly. Therefore, LiSiPON appears disadvantageous for EC devices. In LiPSON,

C. Lupo, D. Schlettwein
Institute for Applied Physics and Center for Materials Research (ZfM/LaMa)
Justus-Liebig-University Giessen
35392 Giessen, Germany
E-mail: schlettwein@uni-giessen.de

F. Michel, F. Kuhl, Y. Su, M. Becker, A. Polity
Institute of Experimental Physics I and Center for Materials Research (ZfM/LaMa)
Justus-Liebig-University Giessen
35392 Giessen, Germany

 The ORCID identification number(s) for the author(s) of this article can be found under <https://doi.org/10.1002/pssb.202100032>.

© 2021 The Authors. physica status solidi (b) basic solid state physics published by Wiley-VCH GmbH. This is an open access article under the terms of the Creative Commons Attribution-NonCommercial-NoDerivs License, which permits use and distribution in any medium, provided the original work is properly cited, the use is non-commercial and no modifications or adaptations are made.

DOI: 10.1002/pssb.202100032

an increasing sulfur content led to an increase in ionic conductivity without losing transparency. Unfortunately, it was shown that LiPSON partly decomposed to ion-insulating Li_2S and Li_2O phases when forming a solid–electrolyte interphase (SEI) in contact with metallic lithium. Therefore, it cannot be applied in lithium-based batteries.^[22] For other applications based on large-scale fabrication processes, however, LiPSON could be of great advantage because of attractive conductivity at acceptable chemical stability. In some studies it was even claimed that it can be manipulated in air, and showed acceptable function even after 2 years.^[23,24] Therefore, based on a reasonable stability against ambient air in combination with good ionic conductivity and transmittance characteristics, LiPSON might serve as a promising candidate for use in all-solid-state EC windows. As metallic lithium is not present in such EC devices, the detrimental SEI formation that disqualified LiPSON for battery use should not occur.

In the present study, LiPSON layers were prepared by radio frequency (RF) magnetron sputtering under variations of the preparation conditions on commercially produced standard electrodes of WO_x that were sputter deposited onto fluorine tin oxide (FTO) on glass^[21] to study their applicability as a solid electrolyte in EC devices. The chemical composition of LiPSON was confirmed by X-ray photoelectron spectroscopy (XPS). Impedance spectroscopy served to determine the ionic conductivity and the activation energy. Results from LiPSON layers prepared on top of WO_x to form EC half-cells in contact with a liquid electrolyte (Figure 1a) served to test the integrity and function of the WO_x /LiPSON interface. The EC performance and the interfacial contact characteristics were studied by spectroelectrochemical measurements and electrochemical impedance spectroscopy (EIS) dependent on the LiPSON preparation conditions, which were adjusted to yield optimum EC performance. Finally, an all-solid-state stack was established by depositing a layer of vanadium titanium oxide (VTi_yO_z) as storage layer and aluminum-doped ZnO (AZO) as counter contact on top of FTO/ WO_x /LiPSON (Figure 1b). Such all-solid-state device revealed improved EC performance compared with the half-cells with the liquid electrolyte. The all-solid-state device not only preserved the reversible EC switching characteristics of WO_x but also could be switched faster.

2. Experimental Section

LiPSON thin films were prepared by RF magnetron sputtering in a SLS/TWIN 400/1000 (Pfeiffer Vacuum) deposition system onto WO_x on FTO on glass provided by EControl-Glas or, for impedance measurements, onto a plate of soda lime glass. To transfer samples without contact to air, a nitrogen-filled glovebox was connected to the load lock. The samples were mounted at 5.3 cm distance from the sputter target, which was obtained from Sindlhauser Materials and consisted of 70 wt% Li_3PO_4 and 30 wt % Li_2SO_4 . The base pressure of the chamber was in the range of 10^{-7} mbar. An argon flux of 16 sccm was established for all samples and additional fluxes of O_2 of 0 sccm, 9 sccm, or 10 sccm (A, B, C) and of N_2 of 3.2 sccm, 4.8 sccm, or 6.4 sccm (1, 2, 3) were established. Thin films were deposited at 15 W sputter power for 180 min. Sample nomenclature included the preparation

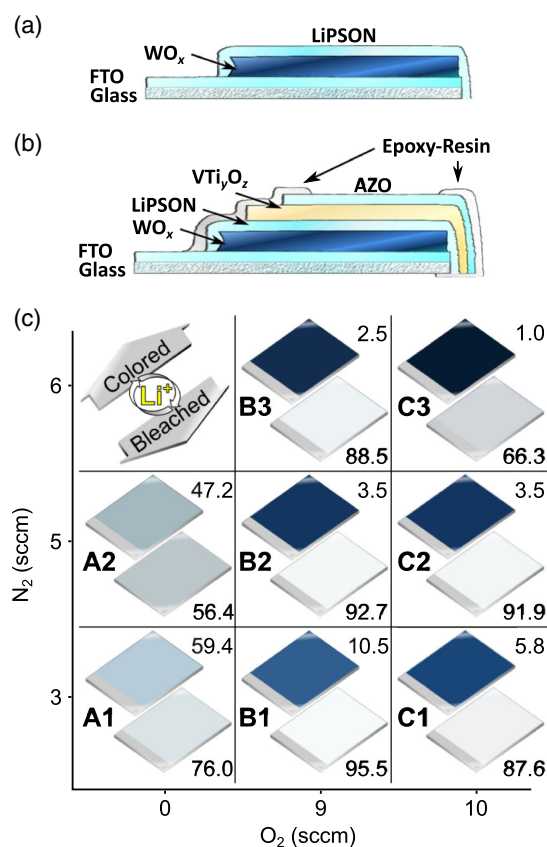


Figure 1. Schematic drawing of the a) EC half-cells and b) the all-solid-state device. c) Influence of the fluxes of O_2 and N_2 during LiPSON preparation (with sample code) on the colors calculated from the recorded spectra at fully colored (-1 V) and bleached states (1 V) observed after 1 h for the EC half-cells in contact to 1 mol L^{-1} LiClO_4 in PC at the respective potential. To the right of each state, the transmittance (in %) at 550 nm is shown.

conditions A, B, C and 1, 2, 3. For the all-solid-state device, a counter electrode layer of VTi_yO_z was prepared from a VTi target (60 wt% vanadium, EControl-Glas) sputtered with 28 sccm argon and 42 sccm O_2 , also at 15 W but for ≈ 15 h on top of a glass/FTO/ WO_x /LiPSON(C2) half-cell. A TCO back contact of AZO directly deposited from an AZO target (2 wt% Al_2O_3 , 98 wt% ZnO, Kurt J. Lesker) with 75 sccm argon at 50 W power for 40 min finalized the stack. The pressure during all depositions was kept in the range from 10^{-3} – 10^{-2} mbar. A summary of all preparation conditions is shown in Table 1.

Before deposition of the LiPSON layer and in case of the all-solid-state device also afterward, additional Li^+ was intercalated into WO_x by use of the three-electrode setup described below. Li^+ was extracted from WO_x during the preparation of the LiPSON layer and during subsequent sputter deposition, directly observed by the loss of blue color during the process. The presence of Li^+ , however, was needed to preserve the functionality of the WO_x layer and ensure overall good performance.^[25] For the all-solid-state device, it is, therefore, mandatory to refill the ion storage before finalizing and sealing the device by VTi_yO_z , AZO, and two-component epoxy resin at

Table 1. Summary of preparation conditions.

Sample	O ₂ [sccm]	N ₂ [sccm]	Ar [sccm]	Target size [inch]	<i>P</i> [W cm ⁻²]	<i>t</i> [min]	<i>d</i> [nm]
A1	0	3.2	16	3	0.33	180	–
A2	0	4.8	16	3	0.33	180	145
B1	9	3.2	16	3	0.33	180	171
B2	9	4.8	16	3	0.33	180	157
B3	9	6.4	16	3	0.33	180	97
C1	10	3.2	16	3	0.33	180	–
C2	10	4.8	16	3	0.33	180	181
C3	10	6.4	16	3	0.33	180	–
VTi _y O _z	42	–	28	4	0.19	900	228
AZO	–	–	75	4	0.62	40	176
LiPSON for all-solid-state device	10	4.8	16	3	0.33	180	197

the open edges (see Figure 1b). To avoid contact with air, subsequent to LiPSON deposition, all samples were transported in hermetically sealed dishes or bags and further handled in a nitrogen-filled glovebox with a water content of less than 0.1 ppm (below detection limit).

To determine the film thicknesses, scanning electron microscopy (SEM) with a Zeiss-Merlin setup with an acceleration voltage of 5 kV, an emission current of 120 pA, and charge compensation with ionized N₂ was used.

Cyclic voltammetric initialization, chronoamperometric measurements, and EC characteristics were determined by an IviumStat (Ivium Technologies) potentiostat coupled with an Evaluation Line (tec5) optical spectrometer system. The EC half-cells were characterized in a three-electrode setup with a platinum wire as counter electrode, a leak-free Ag/AgCl (Harvard Apparatus) as reference electrode, and 1 mol L⁻¹ LiClO₄ (≥ 95%, Sigma-Aldrich) in propylene carbonate (PC, anhydrous, Sigma-Aldrich) as electrolyte. To preserve water-free conditions, the three-electrode setup was mounted in a glovebox into a Zahner PECC-2 cell with a BK7 glass on the one side and the EC half-cell on the other side.^[26] A scan rate of 50 mV s⁻¹ between vertex potentials of -1.2 V and 1.5 V or steps of ± 1 V for 1 h each was used if not otherwise noted. For the all-solid-state device, higher potentials could be used because limitations by the electrochemical stability window of the liquid electrolyte were lifted. We used a potential range of ± 10 V and did not reach the breakthrough voltage of the ion conductor. The spectroelectrochemical measurements were carried out with cells placed in a dark box and reference spectra were obtained by use of the PECC-2 cell filled with electrolyte and a quartz glass instead of the sample for the EC half-cells and an empty box for the all-solid-state cell.

XPS was conducted in a PHI VersaProbe system. X-rays were produced by an Al anode (Al Kα = 1486.6 eV) and the source angle was 45°. During the experiments, charge neutralization on the sample surface was reached by use of an electron gun. The energy scale of the spectra was internally referenced to the carbon 1s signal (C 1s) at 284.8 eV. For bulk analysis

independent of any surface contamination, samples were also measured following in situ argon ion etching with an acceleration voltage of 2 kV.

EIS was carried out by an IM6 workstation (Zahner Elektrik) using a home-made multiplexer and a Eurotherm temperature controller card from room temperature to 368 K in steps of 10 K with an AC voltage of 100 mV amplitude in a frequency range from 0.1 to 8 MHz using 2x2 sandwich structures of 100 nm stainless steel/LiPSON/100 nm stainless steel on soda lime glass substrates deposited by RF sputtering in argon (99.99%), as reported earlier.^[16,27] In the case of the half-cells, the measurements were done in the Zahner PECC-2 cell. The samples were prepared in the same deposition run as the EC samples to ensure identical properties of LiPSON.

The visual representation of the color of the films was calculated from spectra collected during spectroelectrochemical measurements because such calculation was superior to photographs due to the independence on camera type and position, contrast and brightness settings, background, and ambient light, etc. The calculations were carried out according to International Commission on Illumination (CIE) standards by use of an algorithm from the NVIDIA cooperation, in a slightly optimized version based on that previously reported.^[28–30]

3. Results and Discussion

Optimum preparation parameters as established earlier^[20,21] to yield a high ionic conductivity for sputter-deposited LiPSON on glass using a power of 1.1 W cm⁻² and pure N₂ as reactive gas cannot be applied to the present substrates of glass/FTO/WO_x from EControl-Glas without damaging the WO_x top layer. A series of tests revealed that the EC-characteristics of WO_x could only be preserved if the sputtering power was reduced to a maximum of 0.3 W cm⁻². For higher powers, the color of the WO_x layer turned from dark blue to light brown, almost yellow, and lost its otherwise excellent EC switching characteristics, as already observed earlier.^[31,32] The deposition parameters for LiPSON deposited onto WO_x under such softer deposition conditions had to be optimized with respect to the function of LiPSON as ionic conductor at, however, maintained EC activity of WO_x. The LiPSON layers prepared under such modified conditions were characterized by XPS and impedance analysis before spectroelectrochemical characteristics of glass/FTO/WO_x/LiPSON half-cells in contact with a liquid electrolyte (see Figure 1a) and of a glass/FTO/WO_x/LiPSON/VTi_yO_z/AZO (see Figure 1b) EC all-solid-state cell were studied. The different deposition parameters of LiPSON are indicated by a combination of a letter (A, B, and C for 0 sccm, 9 sccm, and 10 sccm O₂, respectively) and a number (1, 2, and 3 for 3.2 sccm, 4.8 sccm, and 6.4 sccm of N₂, respectively).

3.1. Composition of LiPSON Prepared under the Modified Conditions

The chemical composition of LiPSON films was analyzed by XPS. All relevant elements were detected in survey scans. **Figure 2** exemplarily shows spectra of C2, conditions that proved to yield good compatibility to WO_x (see below), and of A2,

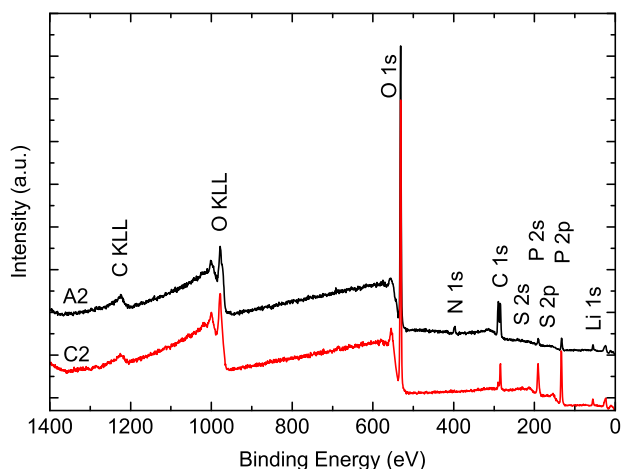


Figure 2. XPS survey spectra for A2 and C2.

conditions close to those established earlier.^[21] Only peaks expected for LiPSON and adventitious carbon were detected. The latter was expected on the sample surface because the samples were briefly exposed to air during transfer from the glovebox to the XPS system and the C 1s signal at 284.8 eV was utilized as reference energy. The N 1s signal for C2 and the sulfur peaks S 2s and S 2p for A1 and C2 can hardly be detected in the survey scan of the surfaces. The atomic concentrations were recorded in the bulk of the films (Figure 3) following Ar⁺ sputtering of the films. By adding oxygen to the plasma during preparation of the LiPSON films (samples B and C), the nitrogen content strongly decreased and the oxygen content increased. Within the oxygen series, the nitrogen content increased with the nitrogen flux and decreased with the partial pressure when the oxygen flux increased, whereas the oxygen content consistently showed an opposite trend. The lithium concentration followed the same trend as nitrogen. The sulfur content was, as also reported earlier, generally quite low, showed a similar trend as nitrogen, but,

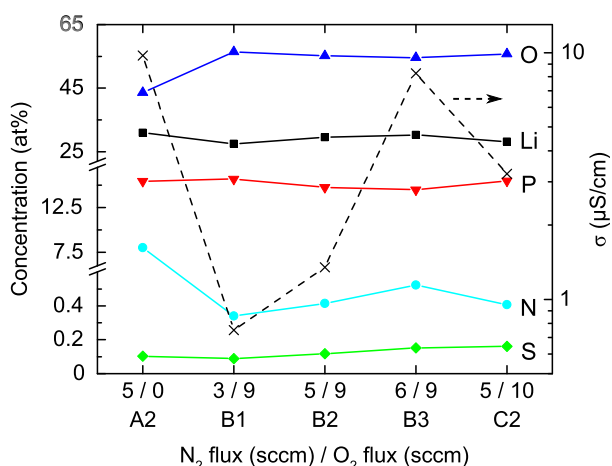


Figure 3. Atomic concentrations for Li, P, S, O, and N from XPS bulk analysis and ionic conductivity derived from temperature-dependent impedance analysis.

in contrast, showed the highest content for the highest fluxes of both, N₂ and O₂.^[21] The concentration of phosphorus followed the same trend as the oxygen content. The elemental composition and the measured ionic conductivity (next paragraph) of A2 as a reference sample are in perfect agreement with published values.^[21,22] The trends within the oxygen series are also in good agreement with the reported correlation between nitrogen content and conductivity.^[33,34] Consistently, the LiPSON films of the B and C series showed a higher oxygen concentration than reported before, as a consequence of the adapted sputtering conditions of an increased oxygen flow. The films covered a range for the ionic conductivity spanning from lower than reported values to the highest values reported for LiPON. The conductivity of B3 with a composition approaching that of LiPON prepared without an additional flux of O₂ (A2) was found to be within the range of values reported earlier.^[21,35] When LiPON was prepared with a comparably low nitrogen concentration, similarly, differing values of the conductivity were obtained, dependent on sputter conditions.^[36,37] Also, the currently found ratios Li/P and Li/O were quite comparable with results reported earlier.^[38]

3.2. Impedance Spectroscopy of the LiPSON Films Prepared under the Modified Conditions

Fast switching times of EC devices require a high ionic conductivity of the electrolyte. Impedance analysis was conducted to discuss the influence of the adapted sputter conditions on the electrical characteristics of the present LiPSON films. By fitting the Nyquist plots to an appropriate equivalent circuit, the ionic conductivity and the activation energy were extracted. Almost all Nyquist plots of the temperature-dependent impedance of the different LiPSON layers look like those in Figure 4a,b and can be fitted well by an equivalent circuit (Figure 4d), consisting of a series resistance R_s (cables, connectors, multiplexer), an inductivity L (mainly from the multiplexer, see Experimental Section), R_{LiPSON} and $\text{CPE}_{\text{LiPSON}}$ (resistance and capacitance of the LiPSON bulk), R_{el} (combined interface resistance of the contacts to stainless steel), and CPE_{el1} and CPE_{el2} (capacitance of the contact interfaces). Constant phase elements (CPEs) were chosen instead of regular capacitances to take care of the dispersive frequency response of the ion conductor. Two independent variables CPE_{el1} and CPE_{el2} were chosen for the two interfaces between LiPSON and stainless steel because of the sequential preparation process, which can lead to asymmetries and, hence, to different frequency responses.^[39,40] Their resistances, however, show no difference in the frequency response and were summarized in one R_{el} , generally needed in thin layers and the corresponding finite-length diffusion. By use of this model, excellent accordance to the measured data was achieved, as shown in Figure 4a,b. This holds even for cases, in which infinite-length diffusion occurs, as, for example, shown in Figure 4b for the sample B1, where R_{el} increases to the MΩ range. The nonblocking behavior seen in Figure 4a was presumably caused by a parasitic electron conductivity as a consequence of incorporated stainless steel particles stemming from the sputtering process of the top electrodes because we only saw this for samples with LiPSON layers less than ≈150 nm thick. Furthermore, the second arc increased with temperature, which

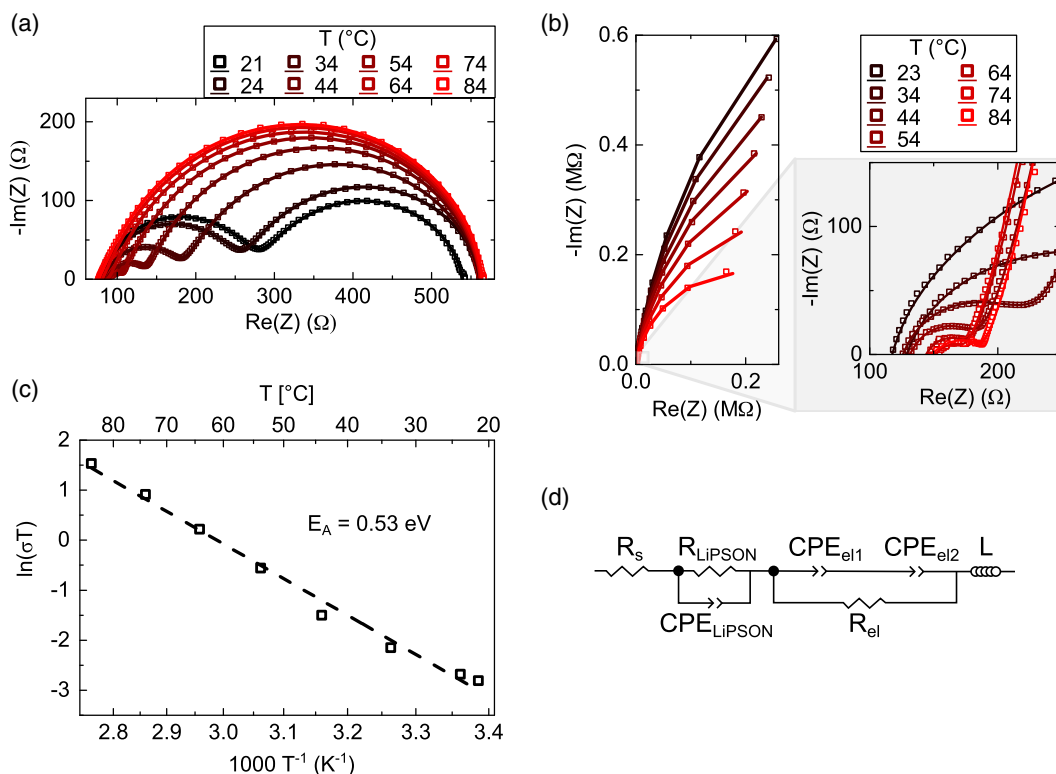


Figure 4. Nyquist plots of the temperature-dependent impedance of samples a) C2 and b) B1. The squares represent measured data points, fits to the data are shown as solid lines. c) Arrhenius plot of the ionic conductivity of sample C2. The dashed line corresponds to a linear fit providing E_A from the slope and σ_{298} by interpolation. d) The equivalent circuit used for fitting the impedance data.

is typical for the conductivity of metals caused by decreasing electron mobility as opposed to a thermally activated ionic conductivity in LiPSON.

The ionic conductivity σ was evaluated by $\sigma = d/(A \cdot R_{\text{LiPSON}})$, where d is the film thickness determined by SEM and A is the area of the metal contact. By use of the Arrhenius-type equation $\ln(\sigma T) = \ln(\sigma_0) - E_A/k_B T$, where σ is the ionic conductivity, σ_0 is a prefactor, T is the absolute temperature, and k_B is Boltzmann constant, the activation energy E_A and the ionic conductivity σ_{298} at room temperature can be extracted (Figure 4c). $E_A = 0.53$ eV was, for example, determined for C2 (other values in Table 2), which falls into the range typically measured for solid electrolytes like LiPON (0.49–0.68 eV), LiSiPON (0.41–0.47 eV), or LiPSON (0.49 eV).^[16,20,21,38,41,42] While E_a seems to increase with increased O_2 flux during deposition (A < B, C) and showed unspecific dependence on the flux of N_2 , σ_{298} significantly decreased with the O_2 flux (A > B, C) and increased with the N_2 flux (1 < 2 < 3). The largest ionic conductivity measured in this series with $9.75 \mu\text{S cm}^{-1}$ (A2) was found only slightly lower than the maximum value of $15.8 \mu\text{S cm}^{-1}$ for LiPSON but still higher than that for LiPON with $3.3 \mu\text{S cm}^{-1}$.^[21,41]

The ionic conductivity of all present layers should be sufficient to serve as solid electrolytes for WO_x EC layers, as can be concluded from a rough estimation. If the device is simplified to a capacitance (WO_x) to be charged over a resistor (LiPSON), the time to load (intercalate) the capacitance up to 90% (τ_{90} , Table 2) can be calculated from $Q(t) = Q_0(1 - \exp(-t/\tau))$ with $\tau = RC$ if the

Table 2. Flux settings for O_2 and N_2 during sputtering of the different LiPSON layers, film thickness d , activation energy E_a , and ionic conductivity σ_{298} at room temperature, the coloration and the bleaching times t_{bc} and t_{cb} in half-cells with a liquid electrolyte, as well as the theoretical time τ_{90} to charge the WO_x layer up to 90% if limited by the resistance of the solid electrolyte.

Sample	O_2 [sccm]	N_2 [sccm]	d [nm]	E_a [eV]	σ_{298} [$S \text{ cm}^{-1}$]	τ_{90} [s]	t_{bc} [s]	t_{cb} [s]
A2	0	4.8	145	0.23	9.75×10^{-6}	0.47	3235	3069
B1	9	3.2	171	0.51	7.50×10^{-7}	7.2	2431	2361
B2	9	4.8	157	0.66	1.35×10^{-6}	3.7	1554	2090
B3	9	6.4	97	0.29	8.25×10^{-6}	0.38	1156	1808
C2	10	4.8	181	0.53	3.23×10^{-6}	1.8	1527	1416
All solid state	10	4.8	197	0.53 ^{a)}	$3.23 \times 10^{-6a)}$	1.9 ^{a)}	38.0	54.1

^{a)}Based on values obtained from identically prepared C2.

resistance R ($1/\sigma_{298}$) of the LiPSON layer and the capacitance C of WO_x as determined by chronoamperometry are used. In this rough estimation, any resistance of tungsten oxide, interfacial resistances, and capacitances were neglected. It can be seen (Table 2) that $\tau_{90} \ll 10$ s would be realistic for all present samples. The LiPSON layer, therefore, would cause only a subtle limitation of the Li^+ -ion movement, which leads to switching times that are more than acceptable for a smart window.

3.3. Impedance Spectroscopy of EC Half-Cells Glass/FTO/ WO_x /LiPSON in Contact with a Liquid Electrolyte

Impedance spectroscopy was also conducted for cells in contact with LiClO_4 in PC using samples prepared within a focused parameter range (A2, B1–3, C2). As seen earlier, the impedance spectra of the LiPSON layers themselves could be fitted by a parallel R-CPE element and it is expected to find similar semicircle features in contact with WO_x and a supporting electrolyte. The impedance response of WO_x has been quite complex and under investigation since several decades. A full description is beyond the scope of this study and can be found in another study, but it should be noted that the present WO_x layers showed the typical impedance characteristics and could be fit well by the extended Randles circuit (purple lines in Figure 5, more details in Figure S2, Supporting Information), which is typically applied for WO_x .^[1,40,43–46] Therefore, two semicircles were expected at high frequencies for the half-cells, the first one for WO_x around $\text{Re}(Z) \approx 35 \Omega$, followed by another one for LiPSON at around $70 \Omega \leq \text{Re}(Z) \leq 100 \Omega$. At low frequencies, starting beyond $\text{Re}(Z) \approx 100 \Omega$, diffusion and bulk transport processes in the electrolyte led to a Warburg or CPE impedance. Just comparing the sizes of the semicircles in the Nyquist plots of the freshly prepared layers in Figure 5a with the trend expected by the evaluated conductivities (Figure 3, Table 2) reveals that sputtering LiPSON on top of WO_x leads to quite different results than expected for the influence of the ionic conductivity measured in the sandwich

structure. The LiPSON layer A2 (highest σ_{298}) should have led to the smallest and B1 (lowest σ_{298}) to the largest semicircle, but in the EC half-cells, A2 showed the largest one and B1 showed (together with B2) the smallest ones. In Figure 5b), details of the measured impedance for A2 and B1 together with that measured for WO_x are shown. The typical increasing imaginary part of WO_x toward $\text{Re}(Z) = 0 \Omega$ is preserved for both EC half-cells, followed by the semicircles for WO_x and LiPSON. For B1, the maximum of the second semicircle was found in the same order of magnitude, strongly overlapping at around $\text{Re}(Z) \approx 75 \Omega$, whereas for A2, the second half-circle was found much larger and more separated with a second maximum at around $\text{Re}(Z) \approx 270 \Omega$ (Figure 5a). Finally, both impedance spectra rose in a 45° slope as expected for semi-infinite diffusion beyond $\text{Re}(Z) \approx 100 \Omega$ (B1) or $\text{Re}(Z) \approx 500 \Omega$ (A2, Figure 5c).

After cycling the EC half-cells ten times between $\pm 1 \text{ V}$, the impedance spectra significantly changed (Figure 5d). Semicircles with much higher impedance were observed, indicating a considerably higher charge transfer resistance, which clearly dominated all other contributions. In the initial state (Figure 5a), the semicircles for all samples except A2 fell within $\text{Re}(Z) \leq 250 \Omega$, increasing by about a factor 100–25 k Ω after cycling (Figure 5d). For A2, this range increased by a factor 2000 from about 500 Ω (Figure 5a) to 1 M Ω (Figure 5d). Also, the sequence of charge transfer impedances (A2 > B3 > C2 > B2, B1, Figure 5a) changed after cycling (A2 > B1 > B2 > C2 > B3, Figure 5d), but the order still did

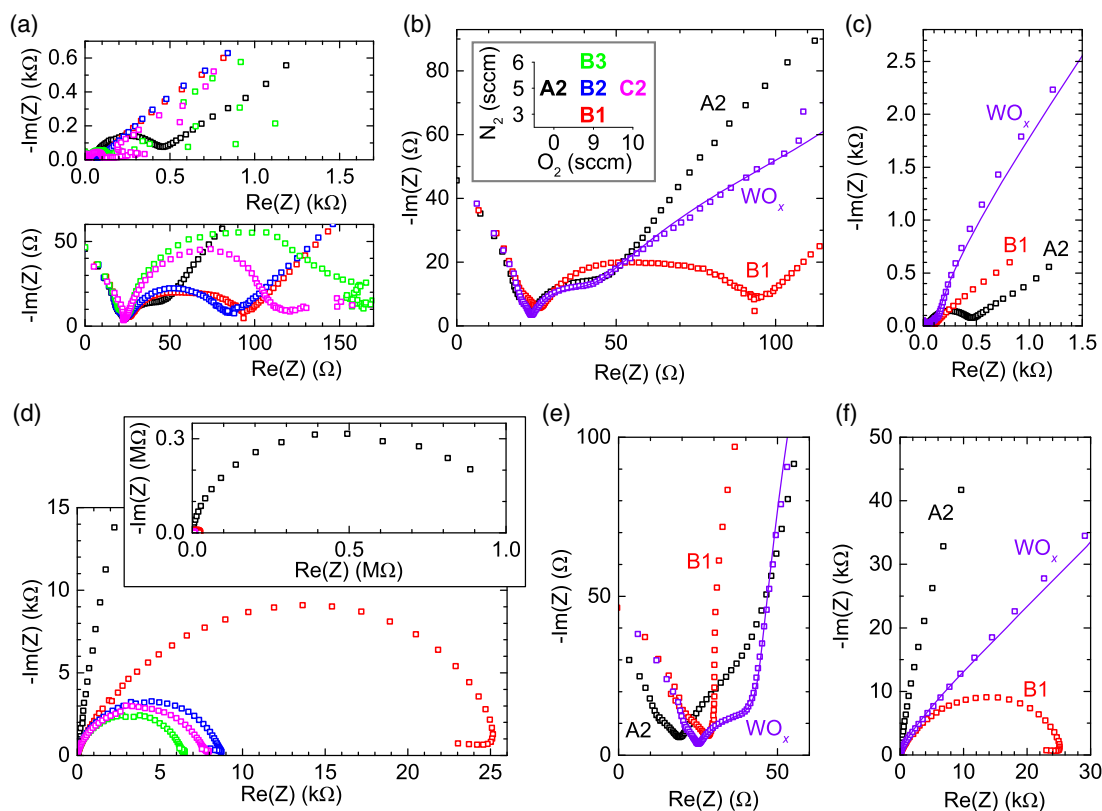


Figure 5. Nyquist plots of the impedance of the a–c) freshly prepared EC half-cells and d–f) after ten cycles at $\pm 1 \text{ V}$. For comparison purposes, the EIS spectra of pure WO_x is also plotted in (b), (c), (e), and (f).

not correlate with the order of LiPSON ionic conductivity ($B1 < B2 < C2 < B3 < A2$, Table 2). The impedance spectra for WO_x equally cycled as the EC half-cells is shown together with the samples with A2 and B1 in Figure 5e,f. The spectra for the cycled pure WO_x did not change much and, in contrast to the spectra for A2 and B1, at $\text{Re}(Z) \geq 40 \Omega$, the bulk transport processes in the electrolyte are still visible.

As no correlation of the observed impedance in half-cells contacted by the liquid electrolyte in Figure 5 was seen with the ionic conductivity measured for the pure LiPSON layers in Figure 3 and Table 2, we conclude that highly resistive interfacial layers must have formed in contact with the liquid electrolyte, in particular during electrochemical cycling. Based on the present experiments alone it could not be decided whether this detrimental interface is located between WO_x and the LiPSON or between the LiPSON and the supporting electrolyte in form of a SEI. From Li^+ -ion batteries, however, it is well known that SEIs play a critical role in the performance of a device and that their influence often changes during cycling.^[22] Therefore, we assign the high resistance and the poor cyclability of the EC half-cells to the formation of an SEI with the liquid electrolyte, which should not come into play in an all-solid-state device.

3.4. Impedance Spectroscopy of the All-Solid-State Device

Impedance spectroscopy of a multilayered all-solid-state device remains a challenging task and an unambiguous assignment of the measured features to physical components of cells is often not possible.^[40] Nevertheless, when compared with the cycled half-cells in contact with a liquid electrolyte (Figure 5d), the temperature-dependent impedance analysis of an all-solid-state device which had been cycled more than 1000 times (Figure 6) allowed a relevant qualitative analysis. The data can be fit by an equivalent circuit similar to that shown in Figure 4d if $(\text{CPE}_{\text{el1}} + \text{CPE}_{\text{el2}})/R_{\text{el}}$ is replaced by an R/CPE group for WO_x and VTi_yO_z each and a CPE element in series for the blocking electrode at lower frequencies. However, the individual contributions are overlapping and cannot be unequivocally assigned to individual physical processes and, therefore, fits

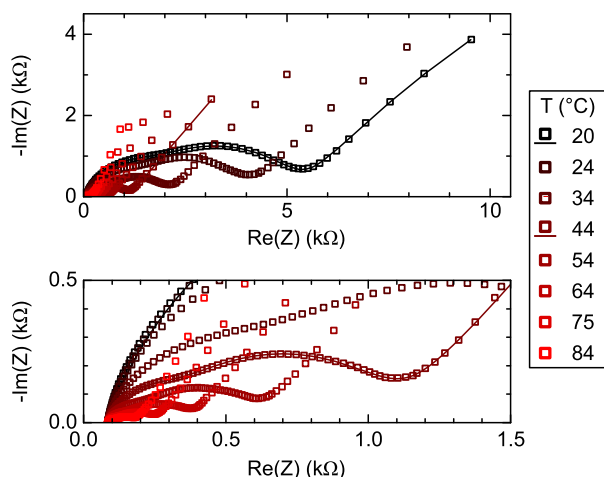


Figure 6. Nyquist plots of the temperature-dependent impedance of an all-solid-state device after more than 1000 cycles.

are only exemplarily shown for 20 and 44 °C. Because all semicircles become smaller with increasing temperature, it can be concluded that the charge transfer in the device is dominated by ion transport. Despite the fact that the ionic mobility in solids is typically found to be much smaller than in electrolyte solutions, the overall impedance for the all-solid-state device is found equal or even slightly smaller than that of the half-cells in contact with a liquid electrolyte (Figure 5d). Further, in contrast to the cycled half-cells in contact with a liquid electrolyte, the all-solid-state device shows a blocking electrode behavior at lower frequencies, expected for purely ionic transport. A detrimental formation of a resistive interface in the contacts of LiPSON with WO_x or VTi_yO_z does not seem to occur in the all-solid-state case, even not after 1000 cycles.

3.5. Visual Appearance of EC Half-Cells Glass/FTO/ WO_x /LiPSON

The visual appearance in the bleached and the colored state of an EC device is one of the most important characteristics. In the application as smart windows, for example, a high transparency in the bleached state is an indispensable property and a low transparency in the colored state determines the quality of function as a shading device. In Figure 1c, graphical representations of the standard red, green, blue color space (sRGB) values (for numerical data, see Table S1, Supporting Information) calculated from spectra measured in the fully colored and fully bleached state of glass/FTO/ WO_x /LiPSON are shown as schematic representations of the electrodes. As a quantitative measure, the values for the transmittance T_{550} at 550 nm are noted on the right of each sample. Directly apparent is a much smaller EC contrast between the fully colored and bleached states of the devices prepared without O_2 (A) or with high fluxes of both O_2 and N_2 (C3). It is caused by low coloration in the case of A and incomplete bleaching in both cases, A and C3. It represents an unacceptable drawback that these devices cannot be fully colored or bleached even within an hour. The best performance in visual appearance was found for samples prepared in the center of the covered parameter range for 5 sccm flow of N_2 and either 9 sccm (B2) or 10 sccm (C2) flux of O_2 . Half-cells with LiPSON prepared under such conditions have a high optical transparency in the bleached state and a strong dark blue visual appearance in the colored state and, correspondingly, show a high difference in T_{550} . By use of a higher N_2 flux (B3, C3), dark blue of the colored state can be further intensified, but the transparency in the bleached state is reduced, in particular at the higher O_2 flux (C3). In contrast, a decreased N_2 flux leads to a less dark colored state (B1, C1) and a slightly increasing transmittance in the bleached state at higher O_2 flux (C1). It should be emphasized that without any O_2 in the sputtering process (A), the samples show just a small optical change during cycling with low transparency in the bleached state and low coloration in the colored state.

3.6. Transmittance Characteristics of EC Half-Cells Glass/FTO/ WO_x /LiPSON

The transmittance spectra (Figure 7) reveal characteristic differences among the samples. From the bleached state (Figure 7a),

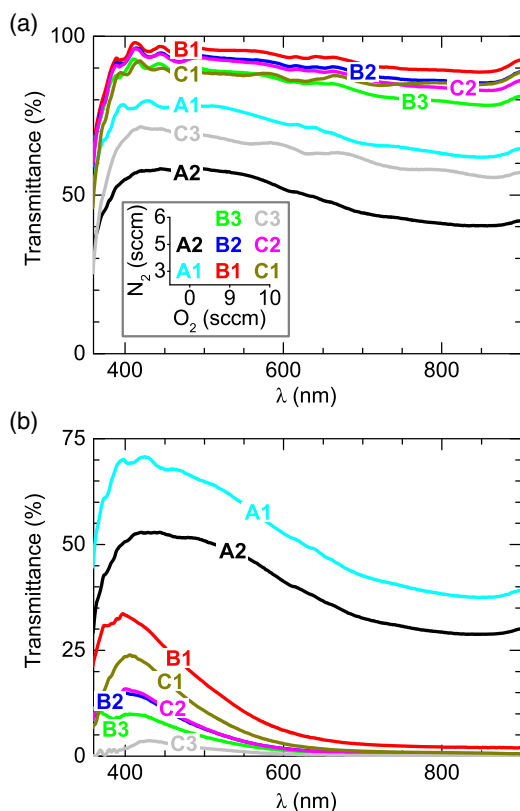


Figure 7. Transmittance spectra of the a) fully bleached and the b) fully colored state of the half-cells under the conditions reported in Table 1.

no apparent spectral differences can be extracted. Spectra of the colored state (Figure 7b), however, indicate a clear influence of the LiPSON deposition conditions (initial states' spectra in SI, Figure S3, Supporting Information). A higher flux of O_2 during preparation leads to significantly more intense coloration $C > B > A$ seen in a decreased transmittance. A higher flux of N_2 during sputter deposition of LiPSON also contributes to increased coloration $3 > 2 > 1$ seen in further reduced transmittance. The decrease in transmittance was particularly strong for wavelengths > 500 nm. A modification of WO_x during the sputter deposition of LiPSON is, thereby, indicated. We assume that the poor performance of type-A half-cells was caused by impact of the LiPSON deposition conditions on the underlying WO_x layer. From a technical point of view, cells are needed with a high transmittance in the bleached state (B1, B2, C1, C2) and a high coloration in the colored state (C3, B3, B2, C2). As an optimum, we find cells B2 and C2, both prepared with a flux of 5 sccm N_2 and 9 sccm or 10 sccm O_2 , respectively.

3.7. Switching Times of EC Half-Cells Glass/FTO/ WO_x /LiPSON

The switching rate of a device is an important parameter. Depending on the area of application, even lower coloration might be acceptable in exchange for higher switching rates. The time-dependent transmittance at 550 nm for potential steps of ± 1 V for 1 h each is shown in Figure 8. Aside from samples A1

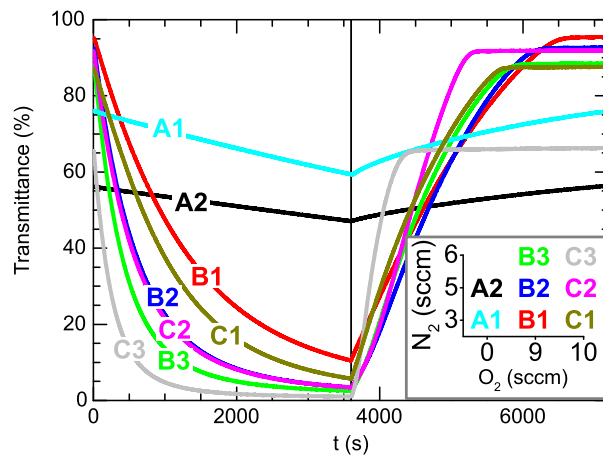


Figure 8. Time-dependent transmittance of EC half-cells at 550 nm for a potential step from 1 V to -1 V on the left and vice versa on the right (the black vertical line denotes the switching point).

and A2, all bleaching processes were finished within 1 h at an applied potential of 1 V, whereas, in the coloration process, most samples show an almost but not quite complete coloration after 1 h at -1 V. Faster bleaching than coloration of WO_x is commonly known and is mainly caused by a barrier at the ion-injecting interface, particularly effective during coloration.^[1] The time needed to reach 90% of the finally achieved transmittance change can be used as a characteristic switching time t for comparison purposes and is easily depicted from measurements like those shown in Figure 8. Sample C3 showed complete coloration and bleaching within 1 h each with a coloration time of $t_{bc} = 750$ s and a bleaching time of $t_{cb} = 599$ s, the shortest among the currently studied samples. However, C3 can just be bleached to a T_{550} value of 74%, leaves a grayish impression (Figure 1), and, thus, cannot be regarded optimum for technical applications. For the samples with optimum spectral characteristics (Section 3.6), B2 and C2, switching times of about 30 min were needed, t_{cb} of 2090 s and 1416 s and t_{bc} of 1554 s and 1527 s, respectively (Table 2). Coloration times t_{bc} were consistently found slightly longer than the bleaching times t_{cb} . Both t_{bc} and t_{cb} decreased for higher fluxes of O_2 ($C < B < A$) or N_2 ($3 < 2 < 1$) during sputter deposition of LiPSON.

As discussed in Section 3.3, the impedance of the cycled EC half-cells did not correspond to the ionic conductivity measured for the LiPSON layers. The overall impedance of half-cells after cycling ($A2 > B1 > B2 > C2 > B3$, Figure 5d), however, perfectly reflected the order of switching times t_{bc} ($A2 > B1 > B2, C2 > B3$, Table 2) with high impedance found for cells of the longest and low impedance for the cells of the shortest t_{bc} . Fitting the large semicircles in Figure 5d) by a simple R-CPE element yielded values between 760 k Ω (A2) and 6.4 k Ω (B3). According to a rough estimation of a time constant (e.g., τ_{90}) proportional to R , such factors would explain a large portion of the significant increase of the switching times t_{bc} and t_{cb} in the half-cells in electrolyte contact compared with τ_{90} , estimated for pure limitation by the resistance of LiPSON. t_{bc} and t_{cb} systematically depended on the LiPSON preparation conditions but did not correlate with its conductivity (Table 2). For the thin layers of less than 200 nm, the resistances are all below

600 Ω , derived from the impedance measurements of the sandwich structures. The much higher resistances calculated from the impedance data of the EC half-cells, therefore, stem from an additional charge transfer resistance.

In summary, sample C2 gave the best spectroelectrochemical results as at almost identical visual appearance (Section 3.5), spectral characteristics (Section 3.6), and t_{bc} , it showed more than 30 % shorter t_{cb} compared with, for example, B2.

3.8. EC Characteristics of an All-Solid-State Cell Glass/FTO/ WO_x/LiPSON/VTi_yO_z/AZO

To demonstrate the use of LiPSON as a solid electrolyte in EC cells and avoid limitations by the interface with a liquid electrolyte, an all-solid-state device was constructed (Figure 1b) with a VTi_yO_z storage layer and an AZO back contact, both sputter deposited subsequently to the LiPSON electrolyte layer (Figure 9). Although the deposition parameters for the VTi_yO_z layer might be improved further, a high quality of the individual layers and the cell stack was obtained. A good material contrast and clear interfaces in SEM indicate an abrupt transition from one material to another without intermixing and all layers appear compact and homogeneous, as shown in Figure 9.

The obtained switching characteristics improved over a significant initialization period of about 150 cycles and then stayed widely constant or slightly improved (see Figure S4 and S5, Supporting Information). From the beginning, the transmittance showed significant changes that stabilized, as shown in Figure 10, with most efficient switching observed at 750 nm. This change and the calculated color obtained from time-dependent spectra are shown during two potential steps (from 10 to -10 V and back to 10 V) for a device after more than 1000 cycles in Figure 10a). The change in transmittance at 750 nm with a ΔT of 38% provides a decent EC contrast. The residual brownish color in the bleached state can be attributed to VTi_yO_z, as can be seen in a comparison with a layer of VTi_yO_z (inset in Figure 10b). The demonstrator all-solid-state EC cell showed a high stability. Even after over 1000 cycles, no degeneration was observed.

The experimental switching times $t_{bc} = 38.0$ s and $t_{cb} = 54.1$ s (Figure 10) are attractively short but are found to be a little longer than the estimated $\tau_{90} = 1.9$ s based on pure limitation by

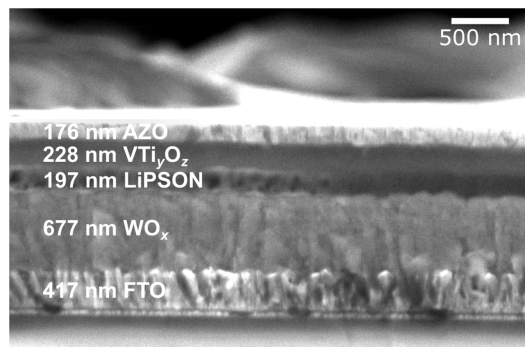


Figure 9. SEM cross section of the all-solid-state device.

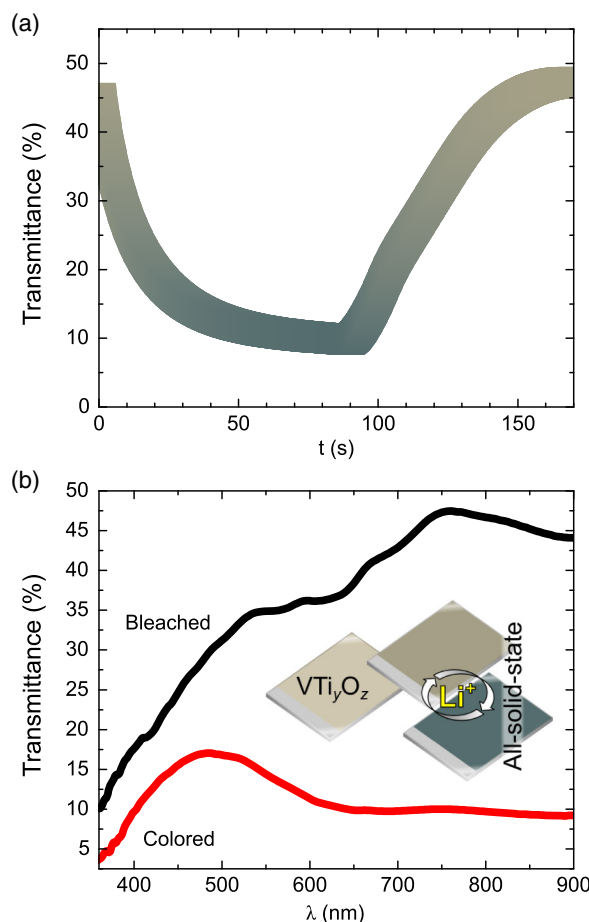


Figure 10. Spectroelectrochemical switching characteristics of an all-solid-state device cycled over 1000 times. a) Time-dependent transmittance at 750 nm during a potential step from 10 V to -10 V and vice versa. The data points are colored by the corresponding calculated RGB values. b) Transmittance spectra for the bleached (black) and colored state (red). The corresponding calculated visual representations as well as that of a VTi_yO_z layer on FTO are shown as inset.

LiPSON ionic conductivity (Table 2), presumably because of factors that were neglected in the simple estimation. Even an as-received WO_x film from EControl-Glas needed a t_{cb} of ≈ 200 s in a three-electrode setup with liquid electrolyte leading, however, to a considerably larger change in transmittance of $\approx 90\%$ at 550 nm (see Figure S1, Supporting Information). A contribution of ion diffusion and/or ionic resistivity within WO_x is, thereby, indicated. Nevertheless, the switching times t_{bc} and t_{cb} in the all-solid-state device were found considerably shorter than for the EC half-cells in contact with a liquid electrolyte with $t > 1000$ s and fit well to the overall lower impedance compared with the half-cells, presumably caused by avoiding SEI formation. Support for this assignment can be drawn from the fast switching and low impedance of the all-solid-state device. Because the preparation conditions of LiPSON for the C2-type half-cell in contact with a liquid electrolyte and the all-solid-state device were identical, the poor performance of the half-cell in contact with the liquid electrolyte could not be caused by any

contact problem at the interface between WO_x and LiPSON, nor by any resistance within LiPSON, but must have been caused by limitations in contact with the liquid electrolyte, indicating formation of an SEI.

4. Conclusion

To investigate the applicability of LiPSON as a solid electrolyte for EC devices, films were sputter deposited onto WO_x substrates and analyzed. Sputtering parameters that were previously optimized toward high ion conductivity could not be applied to depositions on WO_x and had to be adjusted to the chemical sensitivity of WO_x . The chemical composition of LiPSON films prepared under such modified conditions was analyzed by XPS and revealed a new combination of high ionic conductivity for layers with low nitrogen and high oxygen content. The preparation conditions showed a direct influence on the maximum achievable transparency of WO_x in the bleached state and, because of otherwise impractical intercalation times, also on the minimum achievable transparency. Further, a strong dependence of the switching time on the LiPSON preparation conditions was observed for half-cells in contact with a liquid electrolyte, and an additional charge transfer resistance was confirmed by EIS. In comparison with the temperature-dependent EIS measurements of the bare LiPSON layers and results from the all-solid-state device, the increasing resistance for half-cells in contact with a liquid electrolyte was assigned to formation of an SEI. It leads to a high ionic resistance, almost complete blocking of charge transfer, and long coloration/bleaching times for the EC half-cells in contact with a liquid electrolyte. Formation of such a detrimental SEI was not observed in all-solid-state devices, in which LiPSON was contacted by sputter-deposited VTi_yO_z and the stack completed by an AZO counter contact. In such a device, LiPSON performed well with switching times of about 50 s and a large potential window of ± 10 V. We demonstrated stable operation over more than 1000 switching cycles without significant degradation in the spectroelectrochemical characteristics. Further, the proposed stack showed the compatibility of LiPSON with established fabrication technologies for smart windows. Therefore, in contrast to disadvantages in solid-state batteries, because of the formation of a detrimental SEI with metallic lithium, LiPSON can serve as solid electrolyte for all-solid-state EC devices. Because of its high transparency, high ionic conductivity, and reasonable chemical stability against ambient air, LiPSON can be a promising candidate also from a commercial point of view and should be studied further in this context.

Supporting Information

Supporting Information is available from the Wiley Online Library or from the author.

Acknowledgements

The authors are grateful for financial support by the Federal State of Hesse (via "STORE-E" as part of the LOEWE program of excellence), as well as by Deutsche Forschungsgemeinschaft (via the project "SCHL340/19-1" and

via the GRK 2204 "Substitute Materials for sustainable Energy Technologies"), for experimental support by the MiNa laboratory of LaMa/ZfM (University of Giessen) and for technical support by the machine-shop of the Physics Department (University of Giessen). The authors also thank EControl-Glas GmbH & Co. KG (Plauen, Germany) for providing the FTO/ WO_x substrates.

Open access funding enabled and organized by Projekt DEAL.

Conflict of Interest

The authors declare no conflict of interest.

Data Availability Statement

Research data are not shared.

Keywords

electrochromism, impedance spectroscopy, interfaces, ion conductors, spectroelectrochemistry

Received: January 25, 2021

Revised: May 26, 2021

Published online: July 29, 2021

- [1] C. G. Granqvist, *Handbook of Inorganic Electrochromic Materials*, Elsevier, Amsterdam **1995**.
- [2] EControl-Glas GmbH & Co. KG, *Technical data*, <https://www.ec-smartglass.com/assets/Downloads/ec-smart-glass-2-Technical-Data-EN.pdf> (accessed: November 2020).
- [3] H. Wittkopf, M. Dittmar, *Stahlbau* **2012**, *81*, 279.
- [4] A.-L. Larsson, G. A. Niklasson, *Sol. Energy Mater. Sol. Cells* **2004**, *84*, 351.
- [5] C. Sun, J. Liu, Y. Gong, D. P. Wilkinson, J. Zhang, *Nano Energy* **2017**, *33*, 363.
- [6] F. Zheng, M. Kotobuki, S. Song, M. O. Lai, L. Lu, *J. Power Sources* **2018**, *389*, 198.
- [7] P. H. L. Notten, F. Roozeboom, R. A. H. Niessen, L. Baggetto, *Adv. Mater.* **2007**, *19*, 4564.
- [8] K. J. Patel, G. G. Bhatt, J. R. Ray, P. Suryavanshi, C. J. Panchal, *J. Solid State Electron.* **2017**, *21*, 337.
- [9] N. Sbar, M. Badding, R. Budziak, K. Cortez, L. Laby, L. Michalski, T. Ngo, S. Schulz, K. Urbanik, *Sol. Energy Mater. Sol. Cells* **1999**, *56*, 321.
- [10] J. G. Kim, B. Son, S. Mukherjee, N. Schuppert, A. Bates, O. Kwon, M. J. Choi, H. Y. Chung, S. Park, *J. Power Sources* **2015**, *282*, 299.
- [11] A. Sepúlveda, F. Criscuolo, B. Put, P. M. Vereecken, *Solid State Ionics* **2019**, *337*, 24.
- [12] D.-L. Xiao, J. Tong, Y. Feng, G.-H. Zhong, W.-J. Li, C.-L. Yang, *Solid State Ionics* **2018**, *324*, 202.
- [13] I. Y. Cha, S. H. Park, J. W. Lim, S. J. Yoo, Y.-E. Sung, *Sol. Energy Mater. Sol. Cells* **2013**, *108*, 22.
- [14] S. Oukassi, C. Giroud-Garampon, C. Dubarry, C. Ducros, R. Salot, *Sol. Energy Mater. Sol. Cells* **2016**, *145*, 2.
- [15] Y. Xiao, X. Zhong, J. Guo, C. Zhou, H. Zuo, Q. Liu, Q. Huang, Q. Zhang, X. Diao, *Electrochim. Acta* **2018**, *260*, 254.
- [16] Y. Su, J. Falgenhauer, A. Polity, T. Leichtweiß, A. Kronenberger, J. Obel, S. Zhou, D. Schlettwein, J. Janek, B. K. Meyer, *Solid State Ionics* **2015**, *282*, 63.

- [17] P. López-Aranguren, M. Reynaud, P. Głuchowski, A. Bustinza, M. Galceran, J. M. López del Amo, M. Armand, M. Casas-Cabanas, *ACS Energy Lett.* **2021**, 6, 445.
- [18] S. Kalnaus, A. S. Westover, M. Kornbluth, E. Herbert, N. J. Dudney, *J. Mater. Res.* **2021**, 3, 16.
- [19] C. S. Nimisha, G. M. Rao, N. Munichandraiah, G. Natarajan, D. C. Cameron, *Solid State Ionics* **2011**, 185, 47.
- [20] Y. Su, J. Falgenhauer, T. Leichtweiß, M. Geiß, C. Lupó, A. Polity, S. Zhou, J. Obel, D. Schlettwein, J. Janek, B. K. Meyer, *Phys. Status Solidi B* **2017**, 254, 1600088.
- [21] F. Michel, F. Kuhl, M. Becker, J. Janek, A. Polity, *Phys. Status Solidi B* **2019**, 256, 1900047.
- [22] F. Michel, M. Becker, J. Janek, A. Polity, *Phys. Status Solidi B* **2019**, 257, 1900336.
- [23] N. Mascaraque, H. Takebe, G. Tricot, J. L. G. Fierro, A. Durán, F. Muñoz, *J. Non-Cryst. Solids* **2014**, 405, 159.
- [24] N. Mascaraque, J. L. G. Fierro, F. Muñoz, A. Durán, Y. Ito, Y. Hibi, R. Harada, A. Kato, A. Hayashi, M. Tatsumisago, *J. Mater. Res.* **2015**, 30, 2940.
- [25] Ö. D. Coşkun, G. Atak, *Thin Solid Films* **2018**, 662, 13.
- [26] PEC-Cells – PECC-2, <http://zahner.de/products/photoelectrochemistry/pec-cells.html> (accessed: April 2021).
- [27] Y. Su, J. Zhang, S. Shokhovets, A. Polity, B. K. Meyer, *Phys. Status Solidi B* **2017**, 254, 1600424.
- [28] T. Smith, J. Guild, *Trans. Opt. Soc.* **1932**, 33, 73.
- [29] C. Wyman, P. P. Sloan, P. Shirley, *J. Comput. Graph. Tech.* **2013**, 2, 1.
- [30] C. Lupo, F. Eberheim, D. Schlettwein, *J. Mater. Sci.* **2020**, 55, 14401.
- [31] L. Berggren, J. C. Jonsson, G. A. Niklasson, *J. Appl. Phys.* **2007**, 102, 83538.
- [32] D. Dini, F. Decker, E. Masetti, *J. Appl. Electrochem.* **1996**, 26, 647.
- [33] J. Bates, *Solid State Ionics* **1992**, 53–56, 647.
- [34] X. Yu, *J. Electrochem. Soc.* **1997**, 144, 524.
- [35] J. D. LaCoste, A. Zakutayev, L. Fei, *J. Phys. Chem. C* **2021**, 125, 3651.
- [36] L. Le Van-Jodin, A. Claudel, C. Secouard, F. Sabary, J.-P. Barnes, S. Martin, *Electrochim. Acta* **2018**, 259, 742.
- [37] Y. Hamedi Jouybari, F. Berkemeier, A. Schäfer, G. Schmitz, *J. Power Sources* **2018**, 394, 160.
- [38] P. D. Mani, S. Saraf, V. Singh, M. Real-Robert, A. Vijayakumar, S. J. Duranceau, S. Seal, K. R. Coffey, *Solid State Ionics* **2016**, 287, 48.
- [39] L. Le Van-Jodin, F. Ducroquet, F. Sabary, I. Chevalier, *Solid State Ionics* **2013**, 253, 151.
- [40] E. Barsoukov, J. R. Macdonald, *Impedance Spectroscopy: Theory, Experiment, and Applications*, Wiley, Hoboken, NJ **2005**.
- [41] P. Knauth, *Solid State Ionics* **2009**, 180, 911.
- [42] Z. Zheng, S. Song, Y. Wang, *Solid State Ionics* **2016**, 287, 60.
- [43] E. A. Rojas-González, G. A. Niklasson, *J. Appl. Phys.* **2021**, 129, 53103.
- [44] M. Strömme Mattsson, *Solid State Ionics* **2000**, 131, 261.
- [45] C. Bohnke, O. Bohnke, *Solid State Ionics* **1990**, 39, 195.
- [46] C. Ho, *J. Electrochem. Soc.* **1980**, 127, 343.